JACS
JOURNAL OF THE AMERICAN CHEMICAL SOCIETY

ARTICLE

pubs.acs.org/JACS

Tuning the Activity of Pt(111) for Oxygen Electroreduction by Subsurface Alloying

Ifan E. L. Stephens,[†] Alexander S. Bondarenko,[†,§] Francisco J. Perez-Alonso,[†] Federico Calle-Vallejo,[‡] Lone Bech,[†] Tobias P. Johansson,[†] Anders K. Jepsen,[†] Rasmus Frydendal,[†] Brian P. Knudsen,[†] Jan Rossmeisl,[‡] and Ib Chorkendorff[†,*]

[†]Center for Individual Nanoparticle Functionality, Department of Physics, Building 312, Technical University of Denmark, DK-2800 Lyngby, Denmark

[‡]Center for Atomic-scale Materials Design, Department of Physics, Building 311, Technical University of Denmark, DK-2800 Lyngby, Denmark

[§]Center for Electrochemical Sciences, Ruhr-Universität Bochum, Universitätsstrasse 150 NC 4/73, D-44780 Bochum, Germany

Supporting Information

ABSTRACT: To enable the development of low temperature fuel cells, significant improvements are required to the efficiency of the Pt electrocatalysts at the cathode, where oxygen reduction takes place. Herein, we study the effect of subsurface solute metals on the reactivity of Pt, using a Cu/Pt(111) near-surface alloy. Our investigations incorporate electrochemical measurements, ultrahigh vacuum experiments, and density functional theory. Changes to the OH binding energy, ΔE_{OH}, were monitored in situ and adjusted continuously through the subsurface Cu coverage. The incorporation of submonolayer quantities of Cu into Pt(111) resulted in an 8-fold improvement in oxygen reduction activity. The most optimal catalyst for oxygen reduction has an $\Delta E_{OH} \approx 0.1$ eV weaker than that of pure Pt, validating earlier theoretical predictions.

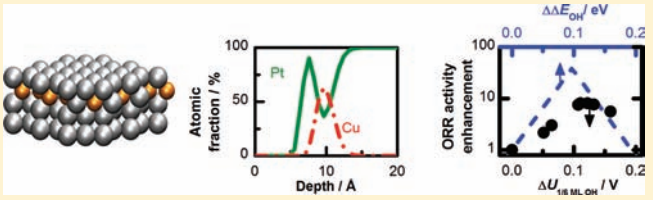

INTRODUCTION

The widespread deployment of electric vehicles would reduce our dependence on fossil fuels and decrease our emissions of greenhouse gases. Polymer electrolyte membrane fuel cells (PEMFCs) are an attractive source of power for such vehicles.[1,2] However, at present, PEMFCs are prohibitively expensive. Further technological advances are needed to decrease the cost and improve the efficiency of the Pt catalysts at the cathode, where the oxygen reduction reaction (ORR) takes place:

$$O_2 + 4H^+ + 4e^- \rightarrow 2H_2O \quad (1)$$

Such breakthroughs would require (a) the replacement of Pt with active and abundant alternatives, or (b) improving the activity of Pt, for instance by alloying it with other metals.[2−4]

To meet this key challenge, a framework was developed to describe and *predict* the overall trends in ORR activity, using density functional theory (DFT) calculations.[5−8] There are at least two to three adsorbed intermediates in the ORR, OH*, OOH*, and O* (where * denotes an adsorbed species). To catalyze the reaction, the binding to all these intermediates needs to be optimized.

On the Pt nanoparticles which catalyze oxygen reduction in PEMFCs, it is widely believed that the active sites are located upon the terraces, in particular the (111) facets.[9,10] More undercoordinated sites bind the intermediates too strongly and would tend to get poisoned. On (111) facets, the overpotential is either due to the hydrogenation of oxygen:[7,8,11]

$$O_2 + H^+ + e^- + * \rightarrow OOH* \quad (2)$$

or the electroreduction of OH* to form water:

$$OH* + H^+ + e^- \rightarrow H_2O + * \quad (3)$$

On Pt(111), the overpotential needed for OH* electrodesorption is marginally higher than that of OOH* formation, which means that step (3) is potential determining.[6,8] It follows that a catalyst which binds to OH* more weakly than Pt(111) would result in a decrease in the overpotential required for OH* reduction. However, it turns out that a surface that binds to OH* more weakly would also bind to OOH* more weakly, in which case OOH* formation, (2), would become potential determining. This is because the stability of O*, OH*, and OOH* all scale linearly.[12,13] Therefore, knowledge of the OH adsorption energy, ΔE_{OH} allows us to describe ΔE_{OOH} and ΔE_O. This is essentially a modern day version of the "Sabatier principle", which states that the most active catalyst for a given reaction should not bind too strongly or too weakly to the reaction intermediates.[14] There are numerous other examples in the recent literature where this principle, corroborated by

Received: December 28, 2010
Published: March 18, 2011

electronic structure theory, has led to the development of quantitative models that describe important trends in gas phase heterogeneous catalysis and electrocatalysis.[5,7,15−22] According to a simple "Sabatier analysis", the most optimal metal catalyst for the ORR has an OH adsorption energy, ΔE_{OH}, ≈ 0.1 eV weaker than Pt(111).[5]

Several strategies have been employed to improve the ORR activity of Pt. These include (a) the utilization of bulk alloys such as Pt_xY, Pt_xSc, Pt_xCo, Pt_xNi, and Pt_xFe;[3,7,23−28] (b) dealloyed $PtCu_x$,[29−31] and (c) the "Pt monolayer" approach, whereby monolayer quantities of Pt are deposited onto a core composed of another, less expensive metal.[32−34] All of these catalysts have a surface overlayer composed entirely of Pt. DFT calculations support the notion that the Pt surface atoms on these catalysts exhibit mildly weaker binding to O* or OH* than pure Pt.[7,29] Indeed, the discovery of Pt_3Y and Pt_3Sc as stable and active catalysts for the ORR was a direct output of the theoretical model, demonstrating its practical application.[7]

Thus far, it has not been possible to probe the descriptor, ΔE_{OH}, experimentally on a number of different surfaces with the same crystal orientation. However, Markovic and co-workers demonstrated that it was possible to estimate the d-band center, ex-situ on a series of polycrystalline Pt_3M alloys, where M = Ni, Co, Fe, Ti, V, using ultraviolet photoemission spectroscopy.[23] The d-band center is a general measure of surface reactivity.[35] A volcano relationship was demonstrated between the d-band center and ORR activity, thus supporting the theoretical model.

On a given crystal facet, the binding of Pt to OH*, OOH*, or O* can be adjusted by two different effects: ligand effects and strain effects.[35−37] Ligand effects occur when the electronic structure of the atoms sitting at the active sites are modified by neighboring atoms of a dissimilar atomic number.[38] For catalysts with a Pt overlayer, ligand effects will be more pronounced when the solute atoms are in the second layer; they are already negligible when the solute atoms are embedded in the fourth atomic layer.[39,40]

Strain effects occur when the catalyst is strained parallel to its surface.[29,39,41] The lattice parameter at the surface will tend toward that of the bulk. Therefore, a change in the bulk composition will result in a corresponding change in the interatomic Pt−Pt distance at the surface. Compressive lattice strain weakens the binding of the Pt surface atoms to adsorbed intermediates, whereas tensile strain will have the opposite effect.

On Pt monolayer catalysts, ligand and strain effects are inseparable.[32−34] This is also the case for bulk Pt alloy catalysts such as Pt_3Y, Pt_3Ni, and Pt_3Co. Their surfaces should always be strained, as their bulk lattice parameters are dissimilar to Pt.[7,42,43] However, the most active forms of Pt_3Co and Pt_3Ni are those with an enrichment of the solute in the subsurface region, suggesting that ligand effects are also important for these catalysts.[25,27]

Strasser and co-workers demonstrated that the high ORR activity of dealloyed $PtCu_x$ could be attributed entirely to strain effects.[29,31] Ex-situ analysis suggested that the catalysts have a thick Pt skin and a Cu-rich core. The smaller lattice parameter of Cu, with respect to Pt, effects a lateral strain to the Pt surface atoms. This, in turn, weakens the binding of the Pt surface atoms to OH*, OOH*, and O*, resulting in a 4−6 fold enhancement in activity over pure Pt.[29] Their study confirmed that bulk lattice strain can be used as a tool to control the ORR activity of Pt. On the contrary, equivalent evidence to demonstrate the role of subsurface alloying has remained elusive.

In the current investigation, we study *near-surface alloys* (NSAs) of Cu/Pt(111). NSAs have unique catalytic properties, distinct from bulk alloys.[21,38,44−47] In a NSA, the solute atoms are only located in the subsurface region, as shown in Figure 1a. Therefore, in a Pt-based NSA, both the surface and the bulk are essentially composed of pure Pt. NSAs have been the focus of several fundamental surface science investigations, conducted under ultrahigh vacuum (UHV) conditions.[21,45−48] To the best of our knowledge, they have not previously been studied for continuous catalytic reactions (i.e., involving turnover) under ambient conditions.

As noted above, there are several reports in the literature where similar, albeit distinct structures have been tested for the ORR. These include (a) well-defined Pt overlayer structures on single crystal substrates, including segregated skin structures and monolayer core−shell structures,[24,32,33] and (b) bulk Pt−Cu alloys in the form of nanoparticles or polycrystalline extended surfaces, where there is always a significant Cu content in the catalyst bulk.[29−31,49] The commonality between these earlier studies is that they were all concerning structures whose core was not composed of pure Pt. This indicates that their activity could at least be partially attributable to bulk lattice strain. Using the Cu/Pt(111) NSA, we aim to elucidate how the catalytic activity of a well-defined single crystal Pt surface can be tuned by the presence of subsurface metals, in the absence of bulk lattice strain.

Our attention was particularly drawn to the Cu/Pt(111) NSA by an investigation by Besenbacher and co-workers.[46] Their DFT calculations suggested that OH* was significantly destabilized on its surface, relative to Pt(111). In the light of the above discussion, this led us to believe that it could have favorable activity for the ORR.

EXPERIMENTAL SECTION

Our experiments capitalize upon the detailed knowledge of the Cu/Pt(111) NSA gained from earlier surface science investigations.[46−48] To prepare and characterize the Cu/Pt(111) NSA in situ, we designed and built a custom setup (further details can be found in the Supporting Information). Briefly, to prepare the desired NSA, up to 1 ML of Cu was electrodeposited onto a Pt(111) single crystal.[50] It was annealed in Ar and H_2 at 400 °C, using an induction heater attached to the cell. On the basis of the earlier studies of this system, the crystal surface should retain its (111) orientation upon the incorporation of subsurface Cu.[46,47] Once the crystal was annealed, the electrode was then characterized in the same cell, using cyclic voltammetry (CV) in 0.1 M $HClO_4$. To measure the ORR activity, the crystal was transferred to a separate cell with a rotating ring disk electrode (RRDE) assembly. The surface structures were independently verified ex-situ, under UHV conditions, using angle resolved X-ray photoelectron spectroscopy (AR-XPS). DFT calculations were used to provide a microscopic interpretation of our experimental results. Full details of the experimental and theoretical methods can be found in the Supporting Information.

RESULTS

Nondestructive depth profiles of the Cu/Pt(111) NSA were obtained using AR-XPS, as shown in the right-hand side of Figure 1. A profile of a Cu/Pt(111) NSA is compared with a pseudomorphic Cu-overlayer on Pt(111)[51,52] and a Cu/Pt(111) surface alloy (SA), where the first layer consists of both Cu and Pt.[47,53] These data should be interpreted qualitatively rather than quantitatively, due to inherent uncertainties in the XPS measurements and the fitting procedures. Nonetheless, the profiles match

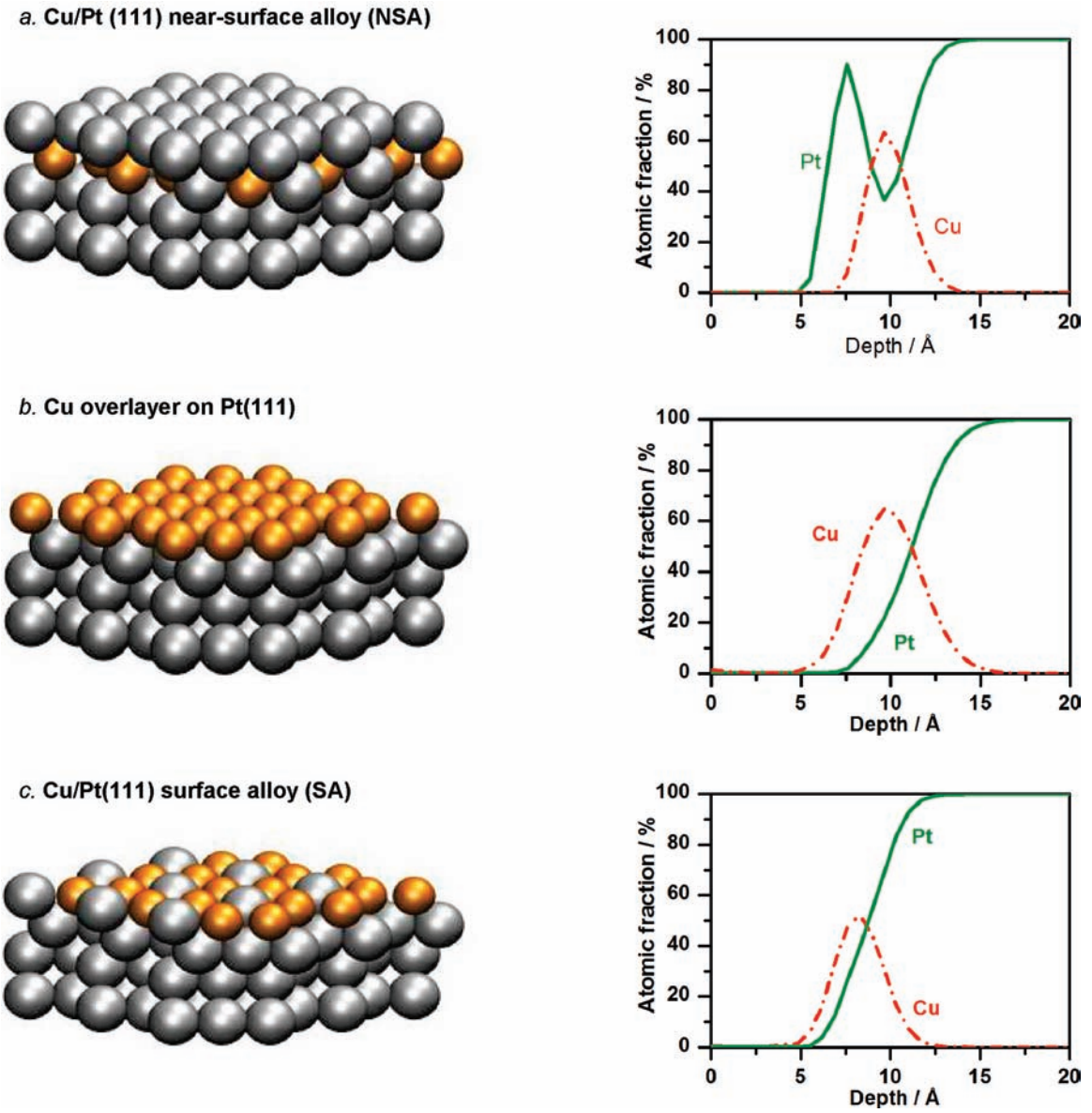

Figure 1. Schematic illustrations (left) and AR-XPS nondestructive depth profiles (right), of (a) the Cu/Pt(111) NSA, with 0.45 ML Cu initially deposited, in comparison to (b) the Cu overlayer on Pt(111), with 1 ML Cu initially deposited and (c) the Cu/Pt(111) surface alloy, with 1 ML Cu initially deposited. In panel a the Cu/Pt NSA had been exposed to ~90 min cycling between 0 and 1 V at 60 °C in O_2-saturated 0.1 M $HClO_4$. The outermost ~5 Å comprised C and O, presumably accumulated from airborne contamination during the transfer from the electrochemical cell, through the laboratory atmosphere to the UHV chamber. The C and O traces have been omitted for clarity.

closely with our expectations, shown in the left-hand side of Figure 1, formed on the basis of previous surface science studies.[46,47,51−53] Moreover, they provide a clear indication that the desired structures are formed.

To quantify the amount of Cu in the near-surface region, in Figure 2 we compare the Cu:Pt intensity ratio, as determined by XPS, for different Cu/Pt(111) NSA samples. The dashed line models the intensity ratio for the case where the amount of Cu initially deposited is equal to the amount of Cu in the second layer. When less than 0.5 ML Cu was initially deposited, there appears to be a 1:1 correspondence between the amount of Cu initially deposited and the final subsurface Cu coverage in the NSA. However, when more than 0.5 ML Cu is initially deposited, the data suggest that some of the Cu is lost from the near-surface region, most likely into the bulk of the crystal. Our observations are consistent with those of Knudsen et al.[46] Their DFT calculations suggested that Cu was stabilized in the second layer of the Cu/Pt(111) NSA, in comparison to deeper layers. On the basis of their XPS results, they estimated that the coverage of Cu in the second layer was 40%, when 1 ML Cu had been deposited initially.

The CVs taken in N_2-saturated 0.1 M $HClO_4$, shown in Figure 3 provide further evidence for the formation of a Pt-skin on the NSA. In the case of the Cu overlayer, there is a sharp anodic peak at ~0.75 V, where Cu dissolves irreversibly into the solution as Cu^{2+}.[52] In the case of the Cu/Pt(111) SA, the Cu dissolution peak is shifted to more anodic potentials, and centered around ~0.85 V. The higher potential required to strip

dx.doi.org/10.1021/ja111690g |*J. Am. Chem. Soc.* 2011, 133, 5485–5491

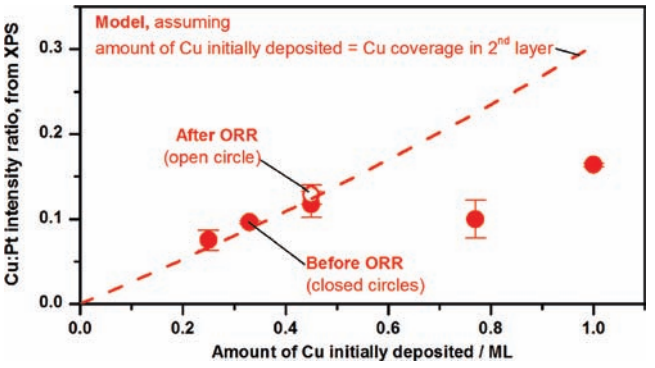

Figure 2. Cu:Pt intensity ratio, from XPS, for the different NSA structures. The analysis was based on the Pt_{4f} and Cu_{2p} photoelectrons emitted at four different angles between 20° and 35° to the sample normal. The Cu:Pt intensity ratio is corrected for the excitation cross section, the mean free path, and the analyzer transmission (full details can be found in the Supporting Information). The error bars show the standard deviations from the data taken at different angles. The dashed line shows the modeled ratio, assuming that the amount of Cu initially deposited (as determined coulometrically), is equal to the subsurface Cu coverage, and that all the Cu is confined to the second layer. The open circle represents the Cu/Pt NSA sample with 0.45 ML Cu initially deposited, after exposure to ~90 min cycling between 0 and 1 V at 60 °C in O_2-saturated 0.1 M $HClO_4$, (the corresponding depth profile is shown in Figure 1a).

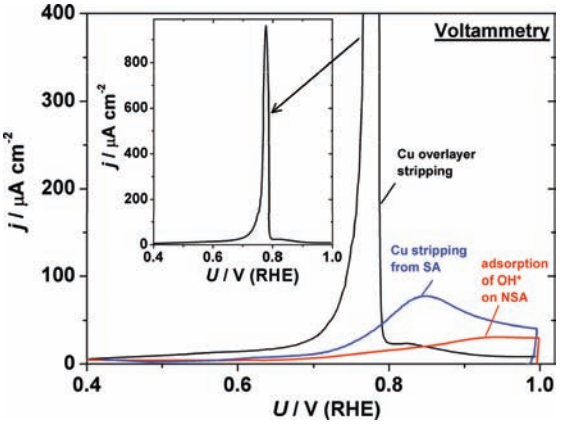

Figure 3. Cyclic voltammograms of the structures shown in Figure 1, in N_2-saturated 0.1 M $HClO_4$, at room temperature, in the absence of Cu^{2+} in solution, $dU/dt = 50$ mV s^{-1}, anodic portion only; in each case 1 ML was deposited initially.

the Cu from the SA suggests that the Cu is stabilized, relative to the overlayer.[54,55] The Cu electro-oxidation features are absent from subsequent cycles; presumably this is because the Cu^{2+} has diffused into the solution. On the contrary, the NSA does not show any features which would suggest that Cu is stripped from the surface. Instead, there is a reversible oxidation feature, unchanged with cycling. This is likely to be due to OH* electrosorption, that is, the reverse of reaction 3.

Cyclic voltammetry in N_2-saturated solution was also used to probe the strength of the interaction of the Cu/Pt(111) NSA with H* and OH*, in situ. Typical CVs of the NSAs with 0−1 ML Cu initially deposited are shown in Figure 4a (a complete set of CVs is shown in the Supporting Information). The shifts in the H* and OH* adsorption peaks show that the presence of Cu in the subsurface destabilizes these adsorbates. Similar features were observed on $Pt_3Ni(111)$ and Pt overlayers on Ru(0001).[24,37] However, the novel feature of the Cu/Pt NSA (and presumably all NSA structures) is the ability to *continuously* adjust the interaction with H* and OH* through the subsurface solute concentration.

The ORR activity was measured for the different NSA surfaces, using CV, as shown in Figure 4b. The activity of Pt(111) reported here compares well with the literature.[24] For each of the catalysts, the current initially shows an exponential increase as the potential is lowered, due to decreasing activation barriers. At higher current densities, the flux of O_2 consumed by the ORR is greater than that which can be sustained by diffusion to the surface. This causes a depletion of O_2 at the electrode, until the current saturates at its diffusion limited value, ~ 6 mA cm^{-2}. The decrease in current below ~0.4 V reflects a change in the reaction pathway, from the complete 4 electron reduction of O_2 to H_2O, to the 2 electron pathway to H_2O_2 (evidence for this is provided in the Supporting Information). In the region of mixed kinetic-diffusion control, between $0.8 < U < 1.0$ V (RHE), there is a pronounced positive shift of up to ~45 mV for the NSAs in comparison with Pt(111), revealing the significantly higher ORR activity of the NSAs.

The ORR activity of the Cu/Pt(111) NSA is stable during the course of the experiment. This observation is consistent with the XPS data shown in Figure 2. The NSA with 0.45 ML Cu initially deposited was analyzed using XPS before and after 90 min of the ORR activity measurement. Within the limits of experimental accuracy, the Cu/Pt ratio remained unchanged.

Over extended time periods, we anticipate that the Cu in the NSA would dissolve into the solution. According to our DFT calculations, the dissolution of the Cu would be thermodynamically favored at potentials above ~0.47 V (as described in more detail in the Supporting Information). We note, in passing, that even the dissolution of bulk Pt is thermodynamically favored above ~1 V.[56] The stability of the Cu in the NSA would be dependent upon the integrity of the Pt overlayer. Once the Cu reaches the surface, it will dissolve easily at high potentials, as shown in the voltammogram of the surface alloy in Figure 3. The kinetics and time scale required for Cu dissolution are challenging to predict. We anticipate that dissolution could either be initiated by OH* or O* induced segregation of Cu to the surface,[57,58] or otherwise due to the dissolution of Pt at steps and other defects.[59] Notably, the data shown in Figure 4 of the Supporting Information show that upon cycling the Cu/Pt(111) NSA to 1.25 V, irreversible changes occur to its voltammogram, suggesting that Cu dissolution may be taking place under these conditions.

DISCUSSION

The overall relationship between the amount of Cu deposited and ORR activity can be deduced from Figure 5a. It is clear that the ORR activity is highly sensitive to the presence of subsurface Cu. Our results confirm that it is possible to optimize the activity of a Pt(111) surface by varying the concentration of Cu in the subsurface region. The curve forms a "volcano", with a broad maximum at ~0.5 ML Cu, representing an 8-fold increase in activity over Pt(111) at 0.9 V. This enhancement is close to the highest recorded to date, that of $Pt_3Ni(111)$.[24]

dx.doi.org/10.1021/ja111690g |J. Am. Chem. Soc. 2011, 133, 5485–5491

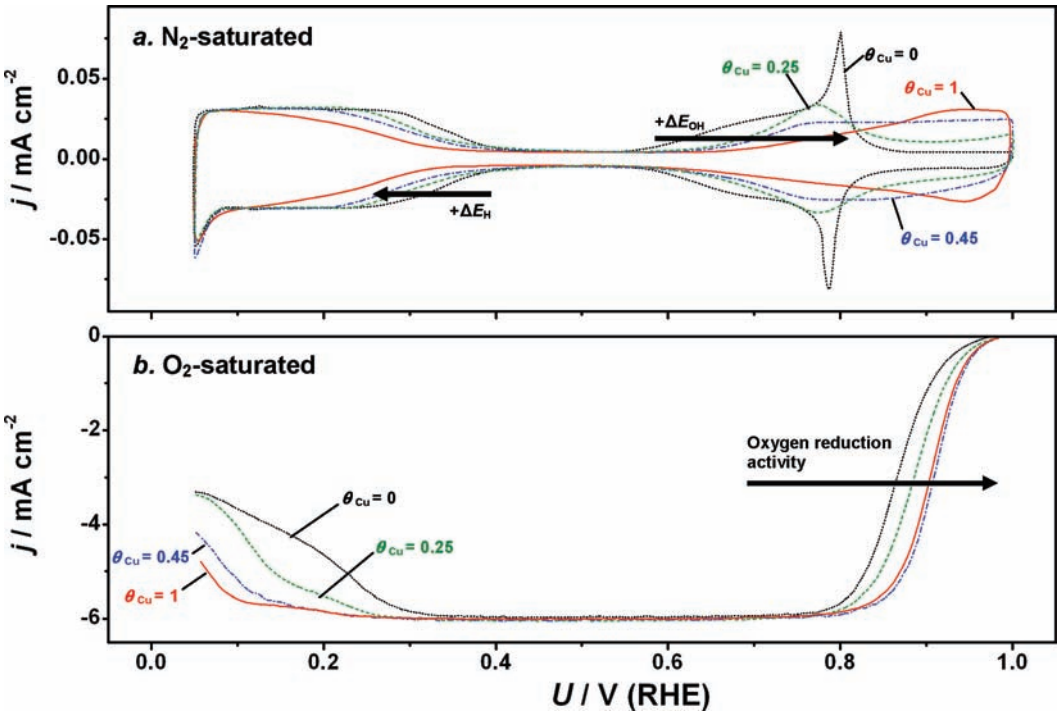

Figure 4. Electrochemical characterization of Cu/Pt(111) NSAs, in comparison with Pt(111), using cyclic voltammetry in 0.1 M $HClO_4$, at dU/dt = 50 mV s^{-1} (a) in N_2-saturated electrolyte; (b) RRDE-voltammograms (anodic scans only) in O_2-saturated electrolyte, taken at 1600 rpm, 60 °C. θ_{Cu} denotes the amount of Cu initially deposited, in monolayers (determined coulometrically, as described in the Supporting Information).

To understand our data in a broader context, it is perhaps more meaningful to relate the activity enhancement to a more universal descriptor, such as the OH binding energy, ΔE_{OH}. Changes to ΔE_{OH}, relative to Pt, that is, $\Delta\Delta E_{OH} = \Delta E_{OH} - \Delta E_{OH}^{Pt}$, can be monitored in situ, through the base voltammograms in N_2, shown in Figure 3a. The shift in potential required to reach $^1/_6$ML coverage of OH*, $\Delta U_{1/6ML\,OH}$, corresponds to the median value of $\Delta\Delta E_{OH}$. On a completely homogeneous Cu/Pt(111) NSA, $\Delta U_{1/6\ ML\ OH} = \Delta\Delta E_{\ OH}$.[6,24]

On Figure 5b, $\Delta U_{1/6ML\,OH}$ is plotted (in black) as a function of the initial amount of Cu electrodeposited onto the crystal. Evidently, $\Delta U_{1/6ML\,OH}$ increases with the Cu content. This trend is reflected in the theoretical plot of $\Delta\Delta E_{OH}$ versus the Cu coverage in the second layer, also shown (in blue) in Figure 5b. Up to ~0.5 ML Cu, the agreement between experiment and theory is good. However, at higher coverages, the large shift in $\Delta\Delta E_{OH}$ that is predicted by DFT is not replicated through $\Delta U_{1/6ML\,OH}$. This is analogous to the trend conveyed by the XPS data shown in Figure 2 and described earlier. Together, these data suggest that it is not possible to obtain a high Cu coverage in the subsurface layer.

It is difficult to ascertain conclusively whether the destabilization of OH* in the NSA arises solely from ligand effects or strain effects. The DFT calculations implicitly assume that the structure is unstrained. The data shown in Figure 5b suggest that the calculations model the experiments well. On that basis, the observed modifications to the binding of the Pt surface could be entirely due to the ligand effect. Even so, there is experimental evidence to suggest that subsurface Cu could introduce some compressive strain to a Pt(111) surface.[48]

Combining the data from Figure 5a and Figure 5b allows us to plot the activity enhancement of the NSA as a function of $\Delta U_{1/6ML\,OH}$, as shown in Figure 5c. The dashed blue line represents the earlier theoretical prediction, based on a simple Sabatier analysis.[5,6] There is a clear maximum in activity for the surface that binds OH* ≈ 0.1 eV weaker than Pt(111), in agreement with earlier theoretical predictions.[5]

We note, from Figure 5c, that the peak activity enhancement from our experiments is around a factor of ~5 lower than that at the peak of the theoretical volcano. This discrepancy could be attributed to kinetic parameters which were not taken into account by the Sabatier analysis.[6] Moreover, it seems likely that the subsurface Cu concentration across the crystal is not uniform. Consequently, $\Delta U_{1/6ML\,OH}$ may not correspond exactly to the $\Delta\Delta E_{OH}$ of the active sites. The most active sites, with the value of $\Delta\Delta E_{OH}$ being closest to the optimum, will dominate the ORR. Nevertheless, a clear trend persists between theory and experiment, as evidenced by the volcano shown in Figure 5c.

The current study complements Strasser and co-workers' investigations of the effect of bulk lattice strain on ORR activity, using dealloyed $PtCu_x$.[29,31] In comparison to dealloyed $PtCu_x$, the Cu/Pt(111) NSAs exhibited slightly higher activity enhancements over pure Pt and also a clear maximum in activity as a function of Cu concentration. It seems that the peak of the volcano can be reached more easily when the solute metal is present in the subsurface. This supports the notion that an important goal in ORR catalysis is the preparation of stable Pt alloy nanoparticles with a high subsurface concentration of the solute component.[25] Moreover, from the data shown in Figure 3, it appears that subsurface Cu is more stable in the NSA than in dealloyed $PtCu_x$.[29,31] One could speculate that our annealing procedure stabilized the solute in the subsurface region, analogous to the observations made for bulk Pt alloys.[60]

dx.doi.org/10.1021/ja111690g |J. Am. Chem. Soc. 2011, 133, 5485–5491

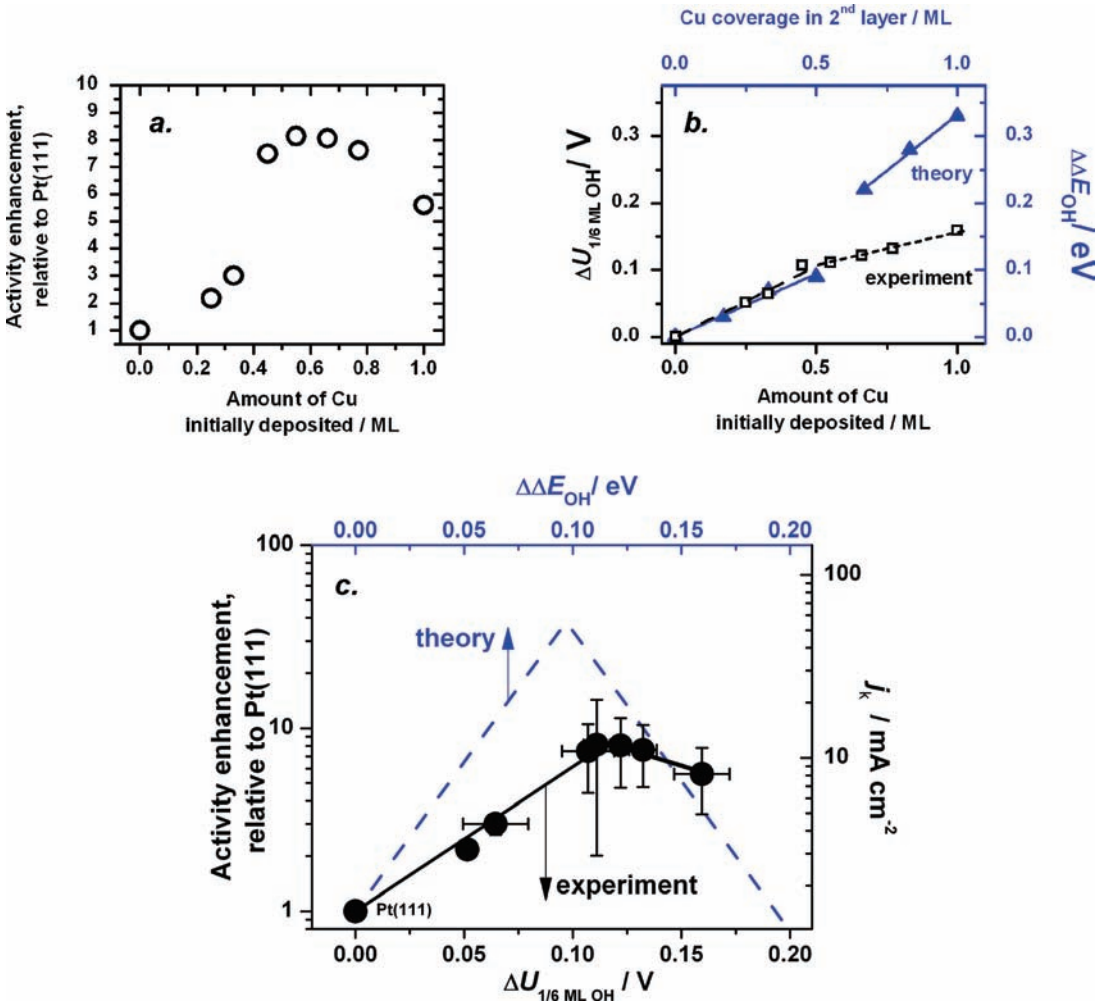

Figure 5. (a) Activity enhancement, relative to Pt(111) at $U = 0.9$ V as a function of the amount of Cu initially deposited, that is $j_{k,NSA}/j_{k,Pt(111)}$, where $j_{k,NSA}$ is the kinetic current density of the Cu/Pt(111) NSA and $j_{k,Pt(111)}$ is the kinetic current density of Pt(111). (b) Experimental and theoretical weakening of OH binding, as a function of Cu content; the linear trendlines were produced using a least-squares fit. (c) Activity enhancement, relative to Pt(111) and kinetic current density, j_k at $U = 0.9$ V versus RHE as a function of $\Delta U_{1/6ML\,OH}$ and $\Delta\Delta E_{OH}$. The circular data points represent experimental data, produced by combining data from *a* and *b*. The data points shown are the mean values, taken from 30 independent measurements, distributed across the entire composition range. The error bars show the standard deviation. The dashed blue line represents earlier theoretical predictions, based upon a simple model using a Sabatier analysis.[5,6] The volcano here is plotted as a function of $\Delta\Delta E_{OH}$ instead of the oxygen adsorption energy, $\Delta\Delta E_O$; the two binding energies, relative to Pt (111), are related by the function $\Delta\Delta E_{OH} \approx 0.5\Delta\Delta E_O$.[13]

CONCLUSION

We have demonstrated that the presence of subsurface 3d metals can weaken the binding of a Pt surface to OH*. This corroborates previous theoretical studies of NSAs.[38,46] We make use of this phenomenon to engineer an ~8-fold enhancement in ORR activity over Pt(111).

We have also shown that it is possible to (a) monitor in situ the binding energy of a simple adsorbate, in this case OH*, on a single crystal surface, (b) tune this binding energy continuously, and (c) use this binding energy as an experimental descriptor for the activity of the surface for a catalytic reaction. We confirm the theoretical prediction that only a slight weakening of the descriptor, ΔE_{OH}, by ~0.1 eV, relative to Pt(111), will lead to optimal activity for the oxygen reduction reaction. To the best of our knowledge, this is the first time that the Sabatier principle has been demonstrated in situ for a continuous catalytic reaction on a well-defined single crystal surface. There is good reason to believe that this principle will continue to be used for the design of yet more active (and ideally abundant) catalysts to meet our future energy requirements.

ASSOCIATED CONTENT

Supporting Information. Full details of the experiments and calculations including the results of additional electrochemical experiments and the raw AR-XPS data. This material is available free of charge via the Internet at http://pubs.acs.org.

AUTHOR INFORMATION

Corresponding Author
ibchork@fysik.dtu.dk

ACKNOWLEDGMENT

Funding by the Danish Strategic Research Council's (DSRC) HyCycle program and SERC project (Grant No. 2104-06-0011)

as well as the Spanish Government's, "Programa Nacional de Movilidad de Recursos Humanos del PN de I+D+I 2008-2011" is gratefully acknowledged. A.S.B. acknowledges additional financial support from the European Union and the MWIFT-NRW (Hightech.NRW competition). The Center for Atomic-scale Materials Design is supported by the Lundbeck Foundation. The Center for Individual Nanoparticle Functionality is supported by the Danish National Research Foundation.

REFERENCES

(1) Eberle, U.; von Helmolt, R. *Energy Environ. Sci.* **2010**, *3*, 689.
(2) Wagner, F. T.; Lakshmanan, B.; Mathias, M. F. *J. Phys. Chem. Lett.* **2010**, *1*, 2204.
(3) Gasteiger, H. A.; Kocha, S. S.; Sompalli, B.; Wagner, F. T. *Appl. Catal., B* **2005**, *56*, 9.
(4) Gasteiger, H. A.; Markovic, N. M. *Science* **2009**, *324*, 48.
(5) Nørskov, J. K.; Rossmeisl, J.; Logadottir, A.; Lindqvist, L.; Kitchin, J. R.; Bligaard, T.; Jonsson, H. *J. Phys. Chem. B* **2004**, *108*, 17886.
(6) Rossmeisl, J.; Karlberg, G. S.; Jaramillo, T.; Nørskov, J. K. *Faraday Discuss.* **2008**, *140*, 337.
(7) Greeley, J.; Stephens, I. E. L.; Bondarenko, A. S.; Johansson, T. P.; Hansen, H. A.; Jaramillo, T. F.; Rossmeisl, J.; Chorkendorff, I.; Nørskov, J. K. *Nat. Chem.* **2009**, *1*, 552.
(8) Tripkovic, V.; Skúlason, E.; Siahrostami, S.; Nørskov, J. K.; Rossmeisl, J. *Electrochim. Acta* **2010**, *55*, 7975.
(9) Greeley, J.; Rossmeisl, J.; Hellman, A.; Nørskov, J. K. *Z. Phys. Chem., Int. J. Res. Phys. Chem. Chem. Phys.* **2007**, *221*, 1209.
(10) Lee, S. W.; Chen, S.; Suntivich, J.; Sasaki, K.; Adzic, R. R.; Shao-Horn, Y. *J. Phys. Chem. Lett.* **2010**, *1*, 1316.
(11) Janik, M. J.; Taylor, C. D.; Neurock, M. *J. Electrochem. Soc.* **2009**, *156*, B126.
(12) Abild-Pedersen, F.; Greeley, J.; Studt, F.; Rossmeisl, J.; Munter, T. R.; Moses, P. G.; Skulason, E.; Bligaard, T.; Nørskov, J. K. *Phys. Rev. Lett.* **2007**, *99*, 016105.
(13) Rossmeisl, J.; Logadottir, A.; Nørskov, J. K. *Chem. Phys.* **2005**, *319*, 178.
(14) Sabatier, P. *Ber. Der Deutsch. Chem. Ges.* **1911**, *44*, 1984.
(15) Logadottir, A.; Rod, T. H.; Nørskov, J. K.; Hammer, B.; Dahl, S.; Jacobsen, C. J. H. *J. Catal.* **2001**, *197*, 229.
(16) Bligaard, T.; Nørskov, J. K.; Dahl, S.; Matthiesen, J.; Christensen, C. H.; Sehested, J. *J. Catal.* **2004**, *224*, 206.
(17) Nørskov, J. K.; Bligaard, T.; Logadottir, A.; Kitchin, J. R.; Chen, J. G.; Pandelov, S.; Stimming, U. *J. Electrochem. Soc.* **2005**, *152*, J23.
(18) Ferrin, P.; Nilekar, A. U.; Greeley, J.; Mavrikakis, M.; Rossmeisl, J. *Surf. Sci.* **2008**, *602*, 3424.
(19) Grabow, L. C.; Mavrikakis, M. *Angew. Chem., Int. Ed.* **2008**, *47*, 7390.
(20) Nørskov, J. K.; Bligaard, T.; Rossmeisl, J.; Christensen, C. H. *Nat. Chem.* **2009**, *1*, 37.
(21) Hansgen, D. A.; Vlachos, D. G.; Chen, J. G. G. *Nat. Chem.* **2010**, *2*, 484.
(22) Neurock, M. *Ind. Eng. Chem. Res.* **2010**, *49*, 10183.
(23) Stamenkovic, V.; Mun, B. S.; Mayrhofer, K. J. J.; Ross, P. N.; Markovic, N. M.; Rossmeisl, J.; Greeley, J.; Nørskov, J. K. *Angew. Chem., Int. Ed.* **2006**, *45*, 2897.
(24) Stamenkovic, V. R.; Fowler, B.; Mun, B. S.; Wang, G. F.; Ross, P. N.; Lucas, C. A.; Markovic, N. M. *Science* **2007**, *315*, 493.
(25) Stamenkovic, V. R.; Mun, B. S.; Arenz, M.; Mayrhofer, K. J. J.; Lucas, C. A.; Wang, G. F.; Ross, P. N.; Markovic, N. M. *Nat. Mater.* **2007**, *6*, 241.
(26) Toda, T.; Igarashi, H.; Uchida, H.; Watanabe, M. *J. Electrochem. Soc.* **1999**, *146*, 3750.
(27) Mayrhofer, K. J. J.; Juhart, V.; Hartl, K.; Hanzlik, M.; Arenz, M. *Angew. Chem., Int. Ed.* **2009**, *48*, 3529.
(28) Chen, S.; Ferreira, P. J.; Sheng, W. C.; Yabuuchi, N.; Allard, L. F.; Shao-Horn, Y. *J. Am. Chem. Soc.* **2008**, *130*, 13818.
(29) Strasser, P.; Koh, S.; Anniyev, T.; Greeley, J.; More, K.; Yu, C. F.; Liu, Z. C.; Kaya, S.; Nordlund, D.; Ogasawara, H.; Toney, M. F.; Nilsson, A. *Nat. Chem.* **2010**, *2*, 454.
(30) Koh, S.; Strasser, P. *J. Am. Chem. Soc.* **2007**, *129*, 12624.
(31) Yang, R.; Leisch, J.; Strasser, P.; Toney, M. F. *Chem. Mater.* **2010**, *22*, 4712.
(32) Zhang, J. L.; Vukmirovic, M. B.; Xu, Y.; Mavrikakis, M.; Adzic, R. R. *Angew. Chem., Int. Ed.* **2005**, *44*, 2132.
(33) Zhou, W. P.; Yang, X. F.; Vukmirovic, M. B.; Koel, B. E.; Jiao, J.; Peng, G. W.; Mavrikakis, M.; Adzic, R. R. *J. Am. Chem. Soc.* **2009**, *131*, 12755.
(34) Adzic, R. R.; Zhang, J.; Sasaki, K.; Vukmirovic, M. B.; Shao, M.; Wang, J. X.; Nilekar, A. U.; Mavrikakis, M.; Valerio, J. A.; Uribe, F. *Top. Catal.* **2007**, *46*, 249.
(35) Bligaard, T.; Nørskov, J. K. *Electrochim. Acta* **2007**, *52*, 5512.
(36) Kitchin, J. R.; Nørskov, J. K.; Barteau, M. A.; Chen, J. G. *Phys. Rev. Lett.* **2004**, *93*, 156801.
(37) Hoster, H. E.; Alves, O. B.; Koper, M. T. M. *ChemPhysChem* **2010**, *11*, 1518.
(38) Kitchin, J. R.; Nørskov, J. K.; Barteau, M. A.; Chen, J. G. *J. Chem. Phys.* **2004**, *120*, 10240.
(39) Schlapka, A.; Lischka, M.; Gross, A.; Kasberger, U.; Jakob, P. *Phys. Rev. Lett.* **2003**, *91*, 016101.
(40) Lischka, M.; Mosch, C.; Gross, A. *Electrochim. Acta* **2007**, *52*, 2219.
(41) Mavrikakis, M.; Hammer, B.; Nørskov, J. K. *Phys. Rev. Lett.* **1998**, *81*, 2819.
(42) Bardi, U.; Beard, B. C.; Ross, P. N. *J. Catal.* **1990**, *124*, 22.
(43) Fowler, B.; Lucas, C. A.; Omer, A.; Wang, G.; Stamenkovic, V. R.; Markovic, N. M. *Electrochim. Acta* **2008**, *53*, 6076.
(44) Greeley, J.; Mavrikakis, M. *Nat. Mater.* **2004**, *3*, 810.
(45) Menning, C. A.; Chen, J. G. *Top. Catal.* **2010**, *53*, 338.
(46) Knudsen, J.; Nilekar, A. U.; Vang, R. T.; Schnadt, J.; Kunkes, E. L.; Dumesic, J. A.; Mavrikakis, M.; Besenbacher, F. *J. Am. Chem. Soc.* **2007**, *129*, 6485.
(47) Andersson, K. J.; Calle-Vallejo, F.; Rossmeisl, J.; Chorkendorff, L. *J. Am. Chem. Soc.* **2009**, *131*, 2404.
(48) Tsay, J. S.; Mangen, T.; Linden, R. J.; Wandelt, K. *Surf. Sci.* **2001**, *482*, 866.
(49) Sarkar, A.; Manthiram, A. *J. Phys. Chem. C* **2010**, *114*, 4725.
(50) Herrero, E.; Buller, L. J.; Abruna, H. D. *Chem. Rev.* **2001**, *101*, 1897.
(51) Leung, L. W. H.; Gregg, T. W.; Goodman, D. W. *Langmuir* **1991**, *7*, 3205.
(52) Markovic, N.; Ross, P. N. *Langmuir* **1993**, *9*, 580.
(53) Andersson, K. J.; Chorkendorff, I. *Surf. Sci.* **2010**, *604*, 1733.
(54) Strasser, P.; Koh, S.; Greeley, J. *Phys. Chem. Chem. Phys.* **2008**, *10*, 3670.
(55) Greeley, J.; Nørskov, J. K. *Electrochim. Acta* **2007**, *52*, 5829.
(56) Pourbaix, M. *Atlas of Electrochemical Equilibria in Aqueous Solutions*; 2nd ed.; National Association of Corrosion Engineers: Houston, TX, 1974.
(57) Abrams, B. L.; Vesborg, P. C. K.; Bonde, J. L.; Jaramillo, T. F.; Chorkendorff, I. *J. Electrochem. Soc.* **2009**, *156*, B273.
(58) Mayrhofer, K. J. J.; Hartl, K.; Juhart, V.; Arenz, M. *J. Am. Chem. Soc.* **2009**, *131*, 16348.
(59) Jinnouchi, R.; Toyoda, E.; Hatanaka, T.; Morimoto, Y. *J. Phys. Chem. C* **2010**, *114*, 17557.
(60) Stamenkovic, V. R.; Mun, B. S.; Mayrhofer, K. J. J.; Ross, P. N.; Markovic, N. M. *J. Am. Chem. Soc.* **2006**, *128*, 8813.